HHS Public Access

Author manuscript

Cell Rep. Author manuscript; available in PMC 2022 January 06.

Published in final edited form as:

Cell Rep. 2021 December 28; 37(13): 110166. doi:10.1016/j.celrep.2021.110166.

Nuclear hormone receptors promote gut and glia detoxifying enzyme induction and protect *C. elegans* from the mold *P. brevicompactum*

Sean W. Wallace[1], **Malcolm C. Lizzappi**[1], **Elif Magemizoğlu**[1], **Hong Hur**[2], **Yupu Liang**[2], **Shai Shaham**[1,3,*]

[1]Laboratory of Developmental Genetics, The Rockefeller University, 1230 York Avenue, New York, NY 10065, USA

[2]CCTS Research Bioinformatics, The Rockefeller University, 1230 York Avenue, New York, NY 10065, USA

[3]Lead contact

SUMMARY

Animals encounter microorganisms in their habitats, adapting physiology and behavior accordingly. The nematode *Caenorhabditis elegans* is found in microbe-rich environments; however, its responses to fungi are not extensively studied. Here, we describe interactions of *C. elegans* and *Penicillium brevicompactum*, an ecologically relevant mold. Transcriptome studies reveal that co-culture upregulates stress response genes, including xenobiotic-metabolizing enzymes (XMEs), in *C. elegans* intestine and AMsh glial cells. The nuclear hormone receptors (NHRs) NHR-45 and NHR-156 are induction regulators, and mutants that cannot induce XMEs in the intestine when exposed to *P. brevicompactum* experience mitochondrial stress and exhibit developmental defects. Different *C. elegans* wild isolates harbor sequence polymorphisms in *nhr-156*, resulting in phenotypic diversity in AMsh glia responses to microbe exposure. We propose that *P. brevicompactum* mitochondria-targeting mycotoxins are deactivated by intestinal detoxification, allowing tolerance to moldy environments. Our studies support the idea that *C. elegans* NHRs may be regulated by environmental cues.

Graphical Abstract

*Correspondence: shaham@rockefeller.edu.

AUTHOR CONTRIBUTIONS

Conceptualization, methodology, validation, formal analysis, investigation, data curation, writing, visualization, supervision, project administration, S.W.W.; conceptualization, methodology, software, formal analysis, resources, writing, supervision, project administration, funding acquisition, S.S.; conceptualization, methodology, validation, investigation, data curation, M.C.L.; software, formal analysis, data curation, H.H.; investigation, data curation, E.M.; methodology, software, formal analysis, resources, data curation, supervision, project administration, Y.L.

SUPPLEMENTAL INFORMATION

Supplemental information can be found online at https://doi.org/10.1016/j.celrep.2021.110166.

DECLARATIONS OF INTERESTS

The authors declare no competing interests.

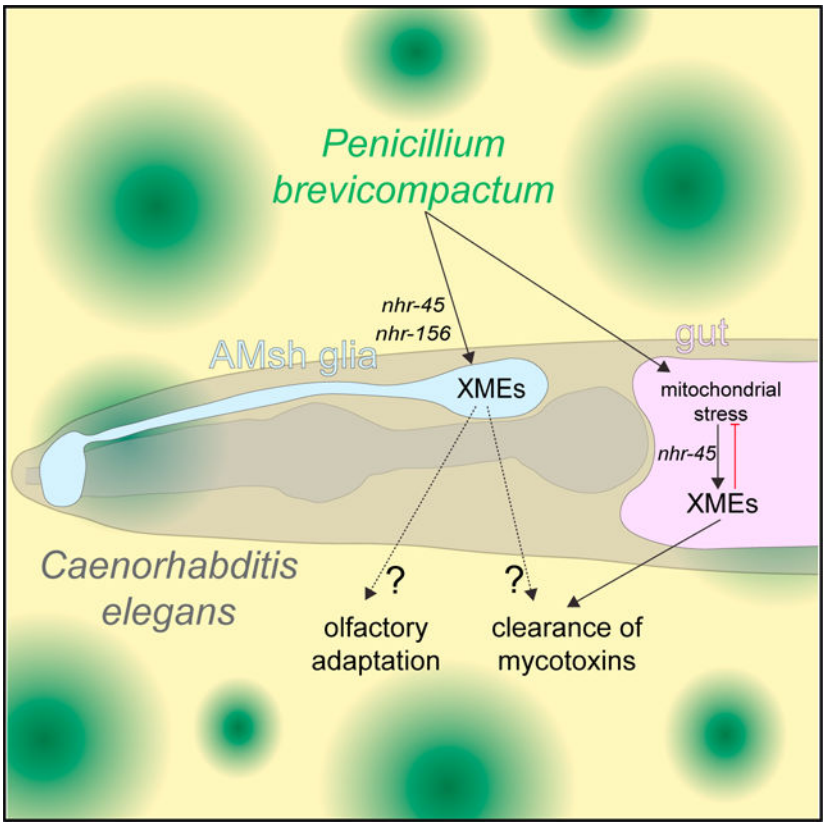

In brief

C. elegans inhabits microbe-rich environments, and there is currently great interest in understanding how they interact with the microbes they encounter in the wild. Wallace et al. describe a transcriptional response that protects *C. elegans* from mitochondrial toxicity when exposed to the fungal mold *Penicillium brevicompactum*.

INTRODUCTION

A number of experimental paradigms have been established to study the interactions between *C. elegans* and model microbial pathogens (Jiang and Wang, 2018; Kim and Ewbank, 2018; Kim and Flavell, 2020; Madende et al., 2020; Radeke and Herman, 2021; Troemel, 2016). Recent work has also explored the interactions between *C. elegans* and the microbial components of its natural substrates in the wild (Schulenburg and Félix, 2017; Zhang et al., 2017), with most of these studies focusing on bacteria. More than 100 mycotoxins have been identified with nematocidal activities (Li et al., 2007), highlighting the notion that, to survive in its habitat, *C. elegans* also possess mechanisms to counter fungi. The *Penicillium* genus includes a large number of abundant fungal species, and the mold *Penicillium brevicompactum* is found naturally in substrates for wild isolates of *C. elegans* (Dirksen et al., 2016). Interactions between *C. elegans* and fungi have not been extensively studied, and effects of *Penicillium* species, in particular, on *C. elegans* are virtually unexplored (Huang et al., 2014; Visagie et al., 2014).

Xenobiotic-metabolizing enzymes (XMEs) are key detoxification proteins that include phase I enzymes of the cytochrome P450 (*cyp*) family, and phase II enzymes of the UDP-glucoronosyltransferase (*ugt*) and glutathione-S-transferase (*gst*) families (Hartman et al., 2021). XME functions have been extensively explored in the mammalian liver, where they play a major role in detoxification. XME responses are induced by the nuclear hormone receptors (NHRs) CAR and PXR after drug exposure (Wallace and Redinbo, 2012). The NHR family in *C. elegans* has undergone massive expansion and sequence diversification (Taubert et al., 2011). NHR genes promote responses to microbe exposure and environmental stress (Jones et al., 2013; Mao et al., 2019; Otarigho and Aballay, 2020; Park et al., 2018; Peterson et al., 2019; Rajan et al., 2019; Shomer et al., 2019; Wani et al., 2021; Ward et al., 2014; Yuen and Ausubel, 2018). Induction of XMEs has also been observed in *C. elegans* in response to exposure to several model pathogens (Engelmann et al., 2011).

Here, we establish an assay to characterize the interactions between *C. elegans* and *P. brevicompactum*. We show that NHRs mediate *P. brevicompactum*-dependent induction of XMEs in the intestine and in glia, and demonstrate a role for NHRs in protecting *C. elegans* from the toxic effects of *P. brevicompactum* exposure.

RESULTS

P. brevicompactum exposure induces expression of stress response genes including XMEs

To establish an assay for investigating interactions between *C. elegans* and fungal molds, we sequenced the internal transcribed spacer rDNA regions (Schoch et al., 2012) of moldy contaminants occurring spontaneously on NGM (nematode growth medium) plates in our laboratory. *Penicillium brevicompactum* (ATCC no. 9056) was identified as a common contaminant, and chosen for further study because, in addition to growing readily on NGM plates suitable for *C. elegans* co-culture, it is found naturally in substrates for wild isolates of *C. elegans* (Dirksen et al., 2016). To characterize transcriptional changes in *C. elegans* following *P. brevicompactum* exposure, whole-animal mRNA was extracted and sequenced from young adult nematodes grown in the presence of the standard food source *E. coli* OP50, with or without *P. brevicompactum* co-culture (see Figure S1A for PCA). We identified 100 genes that are significantly upregulated (fold change > 2, p-adj < 0.05, Tables S1 and S3) and 187 genes that are significantly downregulated (fold change < 0.5, p-adj < 0.05, Tables S2 and S3) following *P. brevicompactum* exposure. Functional analysis using Worm-Cat (Holdorf et al., 2019) showed that more than one-third of the upregulated genes are involved in stress responses (Figure 1A). Statistical enrichment analysis revealed that genes belonging to the stress response sub-categories “detoxification,” “pathogen,” and “heavy metal” are significantly enriched in the dataset of upregulated genes, with genes in the “detoxification” category also showing significant enrichment in the dataset of downregulated genes (Figure 1B). As detoxification genes are the most abundant stress-gene class modulated by *P. brevicompactum* exposure, we focused on these for further characterization.

XMEs are major detoxification proteins encoded by cytochrome P450 (*cyp*), UDP-glucoronosyltransferase (*ugt*), and glutathione-S-transferase (*gst*) gene families (Hartman et al., 2021). Eighteen of the *P. brevicompactum*-induced genes encode XMEs (Figure 1C). To confirm *P. brevicompactum*-dependent induction, and to identify sites of expression, we examined fluorescent transcriptional reporters for six highly induced XMEs. All showed robust induction, validating our RNA sequencing (RNA-seq) data (Figures 1D–1J). XME induction was consistently observed in the intestine, in line with previous reports of detoxification functions in this tissue (Hartman et al., 2021). XME induction was also observed in other tissues, and most consistently in AMsh glial cells, which are components of the major sensory organ in the head of the animal (Singhvi and Shaham, 2019). In these experiments, animals were grown in the presence of *P. brevicompactum* from the L1 stage and scored 2 days later as young adults. XME induction is also observed in adults acutely exposed to *P. brevicompactum*, as demonstrated by *cyp-33C2::GFP* induction within 3 h of exposure in both the intestine and AMsh glia (Figure S1B). Induction of XMEs in AMsh glia is particularly interesting given that XMEs are highly expressed in sustentacular cells, the analogous cell type in the mammalian olfactory epithelium (Heydel et al., 2013).

Overall, our sequencing data demonstrate that exposure of *C. elegans* to *P. brevicompactum* causes significant changes in gene expression, strongly suggesting a biologically meaningful response to this microbe. Furthermore, the significant enrichment of stress response genes, and specifically of detoxification genes, suggests that *P. brevicompactum* may constitute a toxic species for *C. elegans*.

The NHRs *nhr-45* and *nhr-156* are required for XME induction

To investigate the molecular mechanism through which XMEs are induced by *P. brevicompactum*, we initially looked at well-characterized innate immune genes of the p38 MAP kinase pathway (Kim et al., 2002), and at cilia genes that are required for chemosensation (Inglis et al., 2007). Mutations in neither gene class affect XME induction (Figure S2A). We also assessed whether AMsh glia are required for the response in the intestine by using a previously published line in which AMsh glia have been genetically ablated (Bacaj et al., 2008), and found that AMsh glia are not required for the intestinal induction of *cyp-33C2* (Figure S2A).

In light of the established role of CAR and PXR receptors in the induction of XMEs in the mammalian liver (Wallace and Redinbo, 2012), we next screened available *C. elegans nhr* RNAi clones (Table S4) for effects on *P. brevicompactum*-dependent induction of *cyp-33C2::GFP*, an XME reporter we developed (Figure 1E). This screen revealed that *nhr-45* is required for *cyp-33C2* induction in both intestine and AMsh glia, while *nhr-156* is partially required for *cyp-33C2* induction in AMsh glia only. These results were confirmed using a panel of loss-of-function mutants either previously identified or generated in this study (Figures 2A–2C).

The two NHRs we identified function cell autonomously to induce *cyp-33C2* expression. Introduction of an *nhr-45* cDNA under the control of intestine- or AMsh glia-specific promoters into *nhr-45* mutant animals is sufficient to rescue *cyp-33C2::GFP* induction defects in the corresponding tissues (Figure 2D). Interestingly, overexpression of *nhr-156*

(but not overexpression of *nhr-45*) is sufficient to induce expression of *cyp-33C2* even in the absence of *P. brevicompactum* (Figure 2E). It is possible that the *nhr-156* multicopy DNA array generated in these strains bypasses its physiological regulation, resulting in ligand-independent activity. While this result precludes straight-forward interpretation of our rescue experiments, it provides further evidence that *nhr-156* can regulate *cyp-33C2::GFP* induction. Furthermore, *nhr-156* overexpression in AMsh glia induces *cyp-33C2::GFP* expression only in AMsh glia, demonstrating a cell-autonomous function. Consistent with their cell-autonomous functions, expression of *nhr-45* and *nhr-156* is observed in intestinal cells and AMsh glia, as well as in other cell types (Figures 2F and 2G). In these studies, *nhr-45* expression was monitored using a recombineered fosmid encoding a translational fusion to GFP, revealing NHR-45:GFP accumulation in nuclei (Figure 2F). *nhr-156* expression was observed using an *nhr-156* promoter:GFP transcriptional reporter (Figure 2G). Overexpression of *nhr-156* in the intestine, using its endogenous promoter, is sufficient to drive basal expression of *cyp-33C2* in the intestine (Figure S2B). This is perhaps surprising, given that *nhr-156* is not required for *P. brevicompactum*-dependent induction of *cyp-33C2* in this tissue, and suggests that cell-specific physiological regulation of *nhr-156* activity may be compromised when *nhr-156* is overexpressed.

nhr-45 is a major regulator of *P. brevicompactum*-dependent XME induction

To determine if additional XME genes induced by *P. brevicompactum* are dependent on *nhr-45*, we aimed to carry out RNA-seq experiments on *nhr-45* mutant animals. These studies were complicated by our observation (see below) that *P. brevicompactum* at high concentrations is toxic to *nhr-45* mutant animals and causes developmental defects. To circumvent this issue, we took advantage of an *nhr-45* mutant line with a genomically integrated intestine-specific *nhr-45*-expressing transgene (*nsIs910* [*elt-2p:nhr-45*]) that serendipitously exhibits only minimal rescue of *cyp-33C2::GFP* induction in the intestine, but is nonetheless able to rescue the developmental defects. We hypothesized that this strain contains only partial *nhr-45* activity in the intestine, such that it can drive partial expression of target genes in a manner that is sufficient to prevent *P. brevicompactum* toxicity (see below), but still allows *nhr-45*-dependent transcripts to be identified. We predicted that at least some *nhr-45*-dependent transcripts could be identified in this strain, although the extent of this dependence may be underestimated.

By comparing *nhr-45* mutant animals to wild-type animals after exposure to *P. brevicompactum*, we observed that 31 of the 100 *P. brevicompactum*-induced genes we identified require *nhr-45* for their full induction (fold-decrease > 2, p-adj < 0.05 when comparing *nhr-45* mutant with wild-type animals) (Table S1). Of the 18 inducible XMEs we identified, 14 are *nhr-45* dependent (Figure 2H), including *cyp-33C2*, as predicted. We validated the RNA-seq results by assessing induction of *cyp-14A4p::GFP* in the intestine and in AMsh glia, and found that, in both tissues, induction was indeed *nhr-45* dependent (Figure S2C and S2D). With a few exceptions, basal expression of XMEs in the absence of *P. brevicompactum* was not significantly affected in *nhr-45* mutants (Figure 2H). These results show that *nhr-45* is a major regulator of *P. brevicompactum*-dependent XME induction in both the intestine and AMsh glia.

P. brevicompactum is toxic for *nhr-45* mutant animals that fail to induce XMEs in the intestine

Our transcriptome analysis of *P. brevicompactum*-inducible genes revealed strong enrichment for stress response genes involved in detoxification. Furthermore, a large number of mycotoxins have been shown to have nematocidal activities (Li et al., 2007). Together, these observations suggest that *P. brevicompactum* may have toxic effects on *C. elegans*, and that induction of detoxification enzymes may represent a stress response aimed at clearing mycotoxins. Supporting this idea, we observed that *nhr-45* mutants grown on a plate densely seeded with *P. brevicompactum* develop slowly, and in some cases arrest and die at early larval stages. This is in contrast to wild-type animals, which are able to tolerate *P. brevicompactum* exposure (Figures 3A and 3B). Importantly, *nhr-45* mutant animals show normal developmental profiles in the absence of mold (Figures 3A and 3B), indicating that *nhr-45* does not generally affect development. The developmental defect resulting from *P. brevicompactum* exposure can be rescued by restoring *nhr-45* expression in the intestine, but not in AMsh glia (Figure 3C).

nhr-45 was previously shown to regulate XME induction following mitochondrial stress during *Pseudomonas aeruginosa* infection (Mao et al., 2019). To assess whether mitochondrial stress plays a role in *P. brevicompactum* toxicity, we measured *hsp-6p::GFP* expression (Melber and Haynes, 2018). Wild-type animals exposed to *P. brevicompactum* show a modest but significant increase in *hsp-6* expression in the intestine, particularly in the most anterior cells, compared with animals cultured without *P. brevicompactum* (Figures 3D and 3E). *nhr-45* mutant animals, which fail to induce XME expression and show signs of toxicity on *P. brevicompactum*, show massive elevation of *hsp-6::GFP* in the intestine (Figures 3D and 3E). These results suggest that mycotoxins produced by *P. brevicompactum* cause mitochondrial stress, with the anterior intestinal cells being particularly sensitive, perhaps because they are more exposed to the environment, and that this stress can be mitigated by inducing expression of *nhr-45*-dependent detoxifying enzymes. Supporting this idea, we found that applying a known mitochondrial inhibitor, antimycin, phenocopies exposure to *P. brevicompactum*, resulting in *cyp-33C2::GFP* induction in the intestine in an *nhr-45*-dependent manner (Figures 3F and 3G). Furthermore, we observed that *nhr-45* mutants are hypersensitive to the toxic effects of antimycin, consistent with previous observations (Mao et al., 2019). Interestingly, antimycin also induced *cyp-33C2::GFP* in AMsh glia, and this also requires *nhr-45*. However, in contrast to the effect of *P. brevicompactum*, antimycin-dependent induction of *cyp-33C2* in AMsh glia does not require *nhr-156*, suggesting that additional pathways, other than mitochondrial stress pathways, may underlie the effect of *P. brevicompactum* on AMsh glia (Figures 3F and 3G).

Together, our results support a model in which the mold *P. brevicompactum* produces mycotoxins that target mitochondria in the exposed intestinal cells of *C. elegans*, and that *nhr-45*-dependent detoxification pathways are required to clear these toxins and allow animals to tolerate moldy environments.

Natural variation in *nhr-156* underlies phenotypic diversity in AMsh glial transcriptional responses to microbes

Induction of XMEs has been described after exposure of *C. elegans* to several model pathogens (Engelmann et al., 2011). We used the *cyp-33C2::GFP* reporter to assess whether bacterial pathogens also induce XME expression in AMsh glia. We found that the *Serratia marcescens* strain Db10 induces expression of *cyp-33C2* in AMsh glia (as well as in uncharacterized cells near the anterior bulb of the pharynx), and that this induction also requires *nhr-45* and *nhr-156* (Figures 4A and 4B).

The NHR family in *C. elegans* has undergone extensive expansion and diversification, and this has led to the idea that divergent NHRs may have evolved to function as receptors for environmental cues (Arda et al., 2010; Robinson-Rechavi et al., 2005; Sladek, 2011; Taubert et al., 2011). We noticed that there are a number of single-nucleotide polymorphisms (SNPs) in *nhr-156* sequences of several distinct isolates of *C. elegans*, including the Hawaiian strain CB4856, compared with the reference N2 Bristol strain. These SNPs result in predicted coding changes in both the DNA-binding and ligand-binding domains (Figure 4C). To assess whether these changes are functionally important, we carried out a series of experiments to determine whether the Hawaiian variant of *nhr-156* exhibits alterations in its microbe-dependent activity. We initially crossed the *cyp-33C2::GFP* reporter from the N2 background into CB4856, and were surprised to readily isolate recombinant F2 lines in which *cyp-33C2::GFP* induction by *S. marcescens* was lower than observed in N2 (Figure S2A). Partial SNP mapping of the recovered recombinant lines revealed 100% linkage to the Hawaiian variant of *nhr-156* (16 of 16 F2 lines). This result suggests that there is a locus near the Hawaiian *nhr-156* gene that reduces *cyp-33C2::GFP* induction in AMsh glia following *S. marcescens* exposure. The Hawaiian locus responsible for this phenotype failed to complement *nhr-156* loss-of-function alleles, suggesting that *nhr-156* itself is the relevant gene.

To confirm these results, we generated the *nhr-156 (syb2944)* strain in which the N2 *nhr-156* locus is replaced with the Hawaiian variant of the gene. Remarkably, this single-gene substitution phenocopies AMsh glia transcriptional defects observed in the Hawaiian recombinant lines (Figures 4D and 4E). Intriguingly, N2 animals bearing the *nhr-156 (syb2944)* allele still show normal *cyp-33C2::GFP* induction in AMsh glia following exposure to *P. brevicompactum*, demonstrating that the Hawaiian variant of the gene differentially affects the response to different microbes (Figures 4D and 4E).

We also examined three additional *C. elegans* wild isolates with SNPs in the *nhr-156* locus (Figure 4C). Each isolate generated apparently mutant recombinant F2 lines when crossed with the *cyp-33C2::GFP* reporter and exposed to *S. marcescens* (Figure S2A); again with 100% linkage between the phenotype and the variant *nhr-156* locus in each case (16 of 16 F2 lines for each isolate). These recombinant lines also show relatively normal *cyp-33C2* induction following *P. brevicompactum* exposure (Figure 4F). As a control, we obtained two wild isolates that do not harbor codon-changing SNPs in the *nhr-156* locus (JU1088 and JU1171), and found that these strains generate only fully wild-type recombinant F2 lines when crossed with the *cyp-33C2::GFP* marker. Together these results show that divergent sequences in the *nhr-156* gene found in different *C. elegans* strains result in differential

transcriptional responses to microbe exposure, supporting the idea that the expansion and diversification of the NHR family may allow NHRs to act as receptors for specific environmental cues.

DISCUSSION

In this study, we characterized the interaction between *C. elegans* and *P. brevicompactum*, an ecologically relevant species of mold that has been found in substrates that harbor wild isolates of *C. elegans* (Dirksen et al., 2016). A large number of pathogens have been described that infect *C. elegans* and use it as a host. This includes the well-characterized fungal pathogen *Drechmeria coniospora*, whose spores penetrate the cuticle to infect the epidermis (Kim and Ewbank, 2018), as well as *Penicillium marneffei*, which colonizes the intestine (Huang et al., 2014). In both cases, fungal infection results in obvious fungal growth in the nematode host, resulting in death. We have not seen any evidence that *P. brevicompactum* infects *C. elegans* and uses it as a substrate in this way, and instead favor a model in which it is a toxic species rather than an infectious species for *C. elegans*. We propose that *P. brevicompactum* produces mycotoxins that target mitochondria in the intestine and that are normally cleared by XMEs that are induced in a *nhr-45*-dependent manner (Figure 4G). This model is supported by the previous demonstration that *nhr-45* regulates the induction of detoxifying enzymes by mitochondrial stress (Mao et al., 2019), by our observations that *P. brevicompactum* exposure results in mitochondrial stress in the intestine of *nhr-45* mutant animals, and by our findings that the known mitochondrial toxin antimycin phenocopies *P. brevicompactum* exposure, resulting in XME induction in wild-type animals and toxicity in *nhr-45* mutant animals.

Alternative models in which *P. brevicompactum* spores are ingested and infect the nematode cannot be ruled out. Intriguingly, we observed a significant overlap in the genes induced by *P. brevicompactum* exposure to those induced by the pathogens *P. aeruginosa* and *S. marcescens*, both of which colonize the intestine (Fletcher et al., 2019; Engelmann et al., 2011) (Table S5). The implications of this remains unclear, however, as pathogens that infect the intestine also secrete toxins that contribute to their pathogenicity. Our data support a general model of pathogenesis in *C. elegans*, in which microbial toxins disrupt core cellular machineries, and this cellular damage triggers host stress responses (Liu et al., 2014; Melo and Ruvkun, 2012).

XMEs in *C. elegans* have primarily been studied in the intestine (Hartman et al., 2021). In this study we have demonstrated that XMEs are also induced in AMsh glia following *P. brevicompactum* or *S. marcescens* exposure. To our knowledge, this is the first demonstration of such induction in glia. While the implications of microbe-dependent XME induction in glia remain under investigation, it is notable that high levels of XME expression are observed in sustentacular glial cells in the mammalian olfactory epithelium (Heydel et al., 2013), as well as in support cells of insect antennae (Leal, 2013), where they have been proposed to regulate olfactory signaling by modifying odorant molecules. Given the essential role that AMsh glial cells play in regulating chemosensory behavior (Bacaj et al., 2008; Wallace et al., 2016), it is fascinating to speculate that XME induction in AMsh glia may regulate the behavioral adaptations that accompany exposure to pathogens (Kim

and Flavell, 2020). We note, however, that we did not see defects in aversive conditioning to *S. marcescens* in *nhr-45* or *nhr-156* mutants when assessed by lawn-leaving assays (Figure S3B) or defects in survival (Figure S3C). We also checked whether exposure to *P. brevicompactum* affects subsequent chemosensory behavior, and, while *P. brevicompactum* exposure results in reduced chemotaxis to the odorant benzaldehyde, this effect does not depend on *nhr-45* or *nhr-156* (Figure S3D).

The NHR family of *C. elegans* has undergone expansion as well as sequence diversification, particularly in the ligand-binding domain (Robinson-Rechavi et al., 2005). This has led to the idea that environmental cues rather than endogenous endocrine signals may constitute ligands for many NHRs (Sladek, 2011; Taubert et al., 2011). There are numerous examples of NHRs involved in regulating immune or stress responses following microbe or toxin exposure. This includes *nhr-49* and *nhr-8*, which regulate immune responses to *Staphylococcus aureus* and *P. aeruginosa*, respectively (Wani et al., 2021; Otarigho and Aballay, 2020), and *nhr-176* and *nhr-33*/*hizr-1*, which regulate resistance to thiabendazole and cadmium, respectively (Jones et al., 2013; Shomer et al., 2019). Our observation that natural variations in the *nhr-156* gene in wild isolates result in differential transcriptional responses in AMsh glia to microbe exposure supports the idea that NHRs may act as sensors for environmental cues. Future work will investigate the molecular basis for these differences in *nhr-156* activity. It is intriguing that the variants share a common amino acid polymorphism in the ligand-binding domain (Figure 4C), raising the possibility that this change underlies differential activation in response to microbial cues from the environment that act as ligands.

Limitations of the study

While our data support a model in which the mold *P. brevicompactum* produces toxins that cause mitochondrial stress and are toxic for *C. elegans*, and that these toxins are cleared by the induction of XMEs in the intestine, we have not identified the causative mycotoxins. Further work is needed to identify such toxins using biochemical approaches. Our data on the induction of XMEs in glia highlight that this phenomenon occurs, and our data on variation in the glial transcriptional response suggest that *nhr-156* may act as a receptor for environmental cues from microbes. However, the biological significance of the glial XME induction is currently unclear. Further work is needed to elucidate the significance of the glial transcriptional response for detoxification or sensory function.

STAR★METHODS

RESOURCE AVAILABILITY

Lead contact—Further information and requests for resources and reagents should be directed to and will be fulfilled by the lead contact, Shai Shaham (shaham@mail.rockfefeller.edu).

Materials availability—Plasmids and strains generated in this study are available by contacting the lead contact.

Data and code availability—Original RNAseq data files have been deposited at GEO with accession number GEO: GSE183331. This paper does not report original code. Any additional data required to reanalyze the data reported in this paper is available from the lead contact upon request.

EXPERIMENTAL MODELS AND SUBJECT DETAILS

Caenorhabditis elegans—*Caenorhabditis elegans* young adult (approximately 48 h from L1 when grown at 20°C) hermaphrodites were used in this study. Strains were cultured on standard nematode growth media (NGM) plates and fed *E. coli* OP50. Wild type is Bristol N2. The following mutant alleles were generated in this study (see Key Resources Table for a full list of strains used):

nhr-45 (*ns886*) (14 bp deletion in exon1, generated by CRISPR); *nhr-45* (*ns887*) (11 bp insertion in exon 1, generated by CRISPR); *nhr-45* (*ns889*) (7 bp deletion in exon 1, generated by CRISPR); *nhr-156* (*ns865*) (Gln29 > ochre, generated by EMS mutagenesis); *nhr-156* (*syb2944*) (endogenous *nhr-156* gene removed from N2 background and replaced with the Hawaiian variant of the gene – strain created by SunyBiotech).

Penicillium brevicompactum—*Penicillium brevicompactum* (ATCC catalog number 9056) was maintained by culturing on nematode growth media (NGM) plates. Cultures were kept at room temperature for 2 weeks or at 4°C for 2 months. Fresh cultures were created by streaking spores from an existing culture. Frozen stocks were created by scraping material from a plate in M9 buffer and freezing at −80°C with glycerol (final concentration 17%). Mold species were genotyped by scraping material from a plate in M9 buffer, briefly centrifuging to pellet material, and lysing in worm lysis buffer (10 mM Tris pH 8.0, 50 mM KCl, 2.5 mM MgCl2, 0.45% NP-40, 0.45% Tween 20, 0.01% gelatin, 200 μg/mL proteinase K) by incubating at 65°C for 1 h. Genotyping PCRs were performed directly on lysates using ITS, LSU and SSU primers (Schoch et al., 2012).

Serratia marcescens* Db10—Serratia marcescens* Db10 isolate was cultured in liquid by inoculating LB and growing overnight at 37°C 200 rpm. Liquid culture was seeded on NGM plates and allowed to dry at room temperature for *C. elegans* exposure.

METHOD DETAILS

Exposure of *C. elegans* to *P. brevicompactum*—To expose *C. elegans* to *P. brevicompactum*, spores were scraped from a culture plate and added to NGM liquid cultures immediately prior to pouring NGM plates. Plates were left to dry for several days, before being seeded with *E. coli* OP50. Mold spores were calibrated such that approximately 50% of the surface of the plate was covered by mold when the plates were used for *C. elegans* assays (this is considered ‘high density’). Unless otherwise stated, assays were performed by plating synchronized L1s on to moldy plates and scoring phenotypes after 2 days of growth at 20°C.

RNA extraction and sequencing—*C. elegans* were prepared for transcriptome analysis by culturing on plates with or without *P. brevicompactum*, as described above. To avoid

obtaining artifacts due to differences in developmental staging, it is critical that samples are staged correctly. RNA was extracted from samples approximately 48 h from L1 arrest, at which time point the majority of animals had reached the young adult stage. The precise timing was decided empirically for each condition in each experiment, such that some plates were left for up to 52 h if they contained an appreciable number of animals that were still at the L4 stage at the 48-h time point. To overcome the toxicity of *P. brevicompactum* for *nhr-45* mutant animals, we took advantage of the transgenic line *nhr-45* (*ns889*); *nsIs910* (*elt-2*p:*nhr-45* cDNA) that contains a partial rescue of *nhr-45* function in the intestine. This line showed only minimal rescue of *cyp-33C2* induction in the intestine, but showed relatively normal developmental timing on *P. brevicompactum*. We hypothesized that *nhr-45* induces multiple redundantly-acting XME targets, and that the partial restoration of *nhr-45* expression was not sufficient to rescue *cyp-33C2* induction, but was sufficient to prevent toxicity due to its regulation of other targets. We therefore hypothesized that this line would be a useful tool to identify *nhr-45* target genes, albeit with the caveat that we would likely underestimate the extent to which XME expression depends on *nhr-45*. The sequencing data we obtained confirmed this hypothesis; many of the inducible XMEs required *nhr-45* for their full induction, but some still showed partial induction due to the partial *nhr-45* rescue. This line was therefore useful for identifying *nhr-45* target genes without encountering developmental staging problems.

To extract total RNA, animal pellets (approximate size 100 μL after washing in M9 buffer) were suspended in 4x volume Trizol-LS, vortexed for 5 min and subjected to two rounds of freeze-thawing with additional vortexing for 5 min after each thaw. RNA was then isolated using chloroform extraction following the manufacturer's guidelines. Total RNA was then subjected to RNeasy column cleanup with DNAse treatment (QIAGEN). cDNA library preparation and sequencing were as performed by The Rockefeller University Genomics Research Center, using Illumina TruSeq stranded mRNA-Seq library preparation kit with polyA selection, and Illumina NextSeq500. Raw sequencing data has been deposited at GEO with accession number GSE183331.

Differential gene expression analysis—Sequencing data was assessed for quality control using FastQC v0.11.12 (https://www.bioinformatics.babraham.ac.uk/projects/fastqc/) with default parameters. Trimmed fastq files were aligned to WBcel235 using STAR v2.4a aligner with default parameters (Dobin et al., 2013). The alignment results were then evaluated through Qualimap v2.2 (García-Alcalde et al., 2012) to ensure that all the samples had a consistent coverage, alignment rate, and no obvious 5′or 3′ bias. Aligned reads were then summarized through featureCounts on gene (Ensemble gene model Caenorhabditis_elegans.WBcel235.103.gtf). To eliminate the effect of library size, summarized count matrix was normalized through edgeR v 3.28.1 (McCarthy et al., 2012; Robinson et al., 2010). Voom from limma v 3.42.2 was applied to estimate the fold change (Ritchie et al., 2015). A BH-adjusted p value of less than 0.05 ($p\text{-adj} < 0.05$) was used to select genes that have a significant expression change.

Fluorescence microscopy—Imaging was performed using an Axioplan II fluorescence microscope equipped with an AxioCam camera. Images were processed using ImageJ

software. Processing involved orienting the samples, cropping to show the region of interest, and setting the upper and lower intensity thresholds for display. All images in a given experiment were processed in an identical manner.

RNA interference—RNAi by feeding was carried out as described previously (Kamath and Ahringer, 2003), with modifications to allow exposure to *P. brevicompactum*. Overnight cultures of *E. coli* HT115 carrying pL4440 vectors targeting specific genes (Ahringer and Vidal libraries) were seeded on to *P.brevicompactum*-NGM plates (described above) supplemented with carbenicillin (25 ug/mL) and IPTG (1 mM). *C. elegans* were added to plates as L1 larvae and scored 48 h later.

Developmental assay for toxicity—Synchronized L1 larvae were plated on NMG plates seeded with *E. coli* OP50, with or without *P. brevicompactum* (see above). Animals were grown at 20°C for 42–44 h, and the percentage of animals at each developmental stage was counted. This time point was chosen because the majority of animals are in the L4 larval stage for wild type animals under normal conditions.

Antimycin treatment—*C. elegans* were plated on to standard NGM plates with *E. coli* OP50 as synchronized L1 larvae and allowed to develop at 20°C. The following day, 500 μL of antimycin A from *Streptomyces sp.* (Sigma-Aldrich) (6.25 μg/mL in M9 buffer) was added to the plate and allowed to diffuse in to the agar. Animals were then assayed after approximately 24 h of exposure.

***Serratia marcescens* lawn-leaving assays—**Assay plates were made by seeding 30 μL of *Serratia marcescens* Db10 culture on to NGM plates and allowing to dry overnight at room temperature. 20 young adults per replicate were picked on to an assay plate, and the percentage of animals occupying the lawn was calculated at each time point. At least 3 replicates were run for each condition, and data is presented as the mean occupancy of the lawn at each time point.

QUANTIFICATION AND STATISTICAL ANALYSIS

Induction of GFP reporter genes—In some experiments, induction of GFP reporter genes was quantified by scoring the percentage of animals that show visible GFP expression, when assessed by eye using a dissecting microscope. In these experiments, 3 independent replicates were carried out, with at least 30 animals scored blindly per condition per replicate. For rescue experiments, only animals expressing the rescue array, as determined by the presence of the co-injection marker, were scored. Data is presented as the mean of the percentage of animals that show induction across replicates. Significance values were calculated using t-test, for single comparisons, or ANOVA for multiple comparisons. *p*-values and details of the comparisons performed are indicated in the figure legends.

In other experiments, induction of GFP reporter genes was quantified by measuring fluorescence intensity. 3 independent replicates were carried out, with at least 20 animals per replicate. Animals were imaged at high magnification on an Axioplan II fluorescence microscope (see Method Details above), with identical imaging parameters for every sample in a given experiment. Images were then analyzed blindly using ImageJ software. For each

animal, a region of interest was defined and mean pixel intensity was measured. Background subtraction was performed by measuring the mean pixel intensity of a corresponding background region. For each condition in a given experiment, the mean intensity value of all individual animals was calculated. This value was normalized to the corresponding wild-type control in the experiment. Data is presented mean of the normalized fluorescence intensity across the 3 independent replicates. Significance values were calculated using t test, for single comparisons, or ANOVA for multiple comparisons. p values and details of the comparisons performed are indicated in the figure legends.

Developmental assay for toxicity—To assess developmental timing, the percentage of animals at each developmental stage (young adult, larval stage 4, or larval stages 1–3) was scored. 3 independent replicates were carried out, with at least 80 animals scored blindly per condition per replicate. For rescue experiments, only animals expressing the rescue array, as determined by the presence of the co-injection marker, were scored. Data is presented as the mean percentage of animals at each stage across the 3 replicates. Significance values were calculated for the larval stage 4 (L4) category, as this is the stage that the majority of animals develop to under wild-type conditions. Significance values were calculated using ANOVA for multiple comparisons. p-values and details of the comparisons performed are indicated in the figure legends.

Differential gene expression analysis—Full details of the processing of raw sequence files is described above in Method Details section. To calculate significant fold changes, voom from limma v 3.42.2 was applied (Ritchie et al., 2015). A BH-adjusted p-value of less than 0.05 ($p\text{-adj} < 0.05$) was used to select genes that have a significant expression change.

Supplementary Material

Refer to Web version on PubMed Central for supplementary material.

ACKNOWLEDGMENTS

We thank Shaham lab members for helpful discussions and the Rockefeller University Genomics Resource Center for outstanding technical support. Some strains were provided by the CGC, which is funded by NIH Office of research Infrastructure Programs (P40 OD010440). We thank the National Bio-resource Project (NBRP), Cornelia Bargmann, Jonathan Ewbank, and Howard Hang for strains. S.W.W. was a William N. and Bernice E. Bumpus Foundation postdoctoral fellow. This work was supported in part by NIH grant R35 NS105094 to S.S.

REFERENCES

Arda HE, Taubert S, MacNeil LT, Conine CC, Tsuda B, Gilst MV, Sequerra R, Doucette-Stamm L, Yamamoto KR, and Walhout AJM (2010). Functional modularity of nuclear hormone receptors in a *Caenorhabditis elegans* metabolic gene regulatory network. Mol. Syst. Biol 6, 367. [PubMed: 20461074]

Bacaj T, Tevlin M, Lu Y, and Shaham S (2008). Glia are essential for sensory organ function in *C. elegans*. Science 322, 744–747. [PubMed: 18974354]

Dirksen P, Marsh SA, Braker I, Heitland N, Wagner S, Nakad R, Mader S, Petersen C, Kowallik V, Rosenstiel P, et al. (2016). The native microbiome of the nematode *Caenorhabditis elegans*: gateway to a new host-microbiome model. BMC Biol. 14, 38. [PubMed: 27160191]

Dobin A, Davis CA, Schlesinger F, Drenkow J, Zaleski C, Jha S, Batut P, Chaisson M, and Gingeras TR (2013). STAR: ultrafast universal RNA-seq aligner. Bioinformatics 29, 15–21. [PubMed: 23104886]

Engelmann I, Griffon A, Tichit L, Montañana-Sanchis F, Wang G, Reinke V, Waterston RH, Hillier LW, and Ewbank JJ (2011). A comprehensive analysis of gene expression changes provoked by bacterial and fungal infection in *C. elegans*. Plos One 6, e19055. 10.1371/journal.pone.0019055. [PubMed: 21602919]

Fletcher M, Tillman EJ, Butty VL, Levine SS, and Kim DH (2019). Global transcriptional regulation of innate immunity by ATF-7 in *C. elegans*. Plos Genet. 15, e1007830. 10.1371/journal.pgen.1007830. [PubMed: 30789901]

García-Alcalde F, Okonechnikov K, Carbonell J, Cruz LM, Götz S, Tarazona S, Dopazo J, Meyer TF, and Conesa A (2012). Qualimap: evaluating next-generation sequencing alignment data. Bioinformatics 28, 2678–2679. [PubMed: 22914218]

Hartman JH, Widmayer SJ, Bergemann CM, King DE, Morton KS, Romersi RF, Jameson LE, Leung MCK, Andersen EC, Taubert S, et al. (2021). Xenobiotic metabolism and transport in *Caenorhabditis elegans*. J. Toxicol. Environ. Heal Part B 24, 1–44.

Heydel J, Coelho A, Thiebaud N, Legendre A, Bon AL, Faure P, Neiers F, Artur Y, Golebiowski J, and Briand L (2013). Odorant-binding proteins and xenobiotic metabolizing enzymes: implications in olfactory perireceptor events. Anatomical Rec. 296, 1333–1345.

Holdorf AD, Higgins DP, Hart AC, Boag PR, Pazour GJ, Walhout AJM, and Walker AK (2019). WormCat: an online tool for annotation and visualization of *Caenorhabditis elegans* genome-scale data. Genetics 214, 279–294. [PubMed: 31810987]

Huang X, Li D, Xi L, and Mylonakis E (2014). *Caenorhabditis elegans*: a simple nematode infection model for *Penicillium marneffei*. PLoS One 9, e108764. 10.1371/journal.pone.0108764. [PubMed: 25268236]

Inglis PN, Ou G, Leroux MR, and Scholey JM (2007). The sensory cilia of *Caenorhabditis elegans*_revised. Wormbook, 1–22.

Jiang H, and Wang D (2018). The microbial zoo in the *C. elegans* intestine: bacteria, fungi and viruses. Viruses 10, 85.

Jones LM, Rayson SJ, Flemming AJ, and Urwin PE (2013). Adaptive and specialised transcriptional responses to xenobiotic stress in *Caenorhabditis elegans* are regulated by nuclear hormone receptors. PLoS One 8, e69956. 10.1371/journal.pone.0069956. [PubMed: 23922869]

Kamath RS, and Ahringer J (2003). Genome-wide RNAi screening in *Caenorhabditis elegans*. Methods 30, 313–321. [PubMed: 12828945]

Kim DH, and Ewbank JJ (2018). Signaling in the innate immune response. Wormbook, 1–35.

Kim DH, and Flavell SW (2020). Host-microbe interactions and the behavior of *Caenorhabditis elegans*. J. Neurogenet 34, 1–10. [PubMed: 32233839]

Kim DH, Feinbaum R, Alloing G, Emerson FE, Garsin DA, Inoue H, Tanaka-Hino M, Hisamoto N, Matsumoto K, Tan M-W, et al. (2002). A conserved p38 MAP kinase pathway in *Caenorhabditis elegans* innate immunity. Science 297, 623–626. [PubMed: 12142542]

Leal WS (2013). Odorant reception in insects: roles of receptors, binding proteins, and degrading enzymes. Annu. Rev. Entomol 58, 373–391. [PubMed: 23020622]

Li G, Zhang K, Xu J, Dong J, and Liu Y (2007). Nematicidal substances from fungi. Recent Patents Biotechnol. 1, 212–233.

Liu Y, Samuel BS, Breen PC, and Ruvkun G (2014). *Caenorhabditis elegans* pathways that surveil and defend mitochondria. Nature 508, 406–410. [PubMed: 24695221]

Madende M, Albertyn J, Sebolai O, and Pohl CH (2020). *Caenorhabditis elegans* as a model animal for investigating fungal pathogenesis. Med. Microbiol. Immun 209, 1–13.

Mao K, Ji F, Breen P, Sewell A, Han M, Sadreyev R, and Ruvkun G (2019). Mitochondrial dysfunction in *C. elegans* activates mitochondrial relocalization and nuclear hormone receptor-dependent detoxification genes. Cell Metab 29, 1182–1191.e4. [PubMed: 30799287]

McCarthy DJ, Chen Y, and Smyth GK (2012). Differential expression analysis of multifactor RNA-Seq experiments with respect to biological variation. Nucleic Acids Res. 40, 4288–4297. [PubMed: 22287627]

Melber A, and Haynes CM (2018). UPRmt regulation and output: a stress response mediated by mitochondrial-nuclear communication. Cell Res 28, 281–295. [PubMed: 29424373]

Melo JA, and Ruvkun G (2012). Inactivation of conserved *C. elegans* genes engages pathogen- and xenobiotic-associated defenses. Cell 149, 452–466. [PubMed: 22500807]

Otarigho B, and Aballay A (2020). Cholesterol regulates innate immunity via nuclear hormone receptor NHR-8. Iscience 23, 101068. 10.1016/j.isci.2020.101068. [PubMed: 32361270]

Park MR, Ryu S, Maburutse BE, Oh NS, Kim SH, Oh S, Jeong S-Y, Jeong D-Y, Oh S, and Kim Y (2018). Probiotic *Lactobacillus fermentum* strain JDFM216 stimulates the longevity and immune response of *Caenorhabditis elegans* through a nuclear hormone receptor. Sci. Rep-Uk 8, 7441.

Peterson ND, Cheesman HK, Liu P, Anderson SM, Foster KJ, Chhaya R, Perrat P, Thekkiniath J, Yang Q, Haynes CM, et al. (2019). The nuclear hormone receptor NHR-86 controls anti-pathogen responses in *C. elegans*. Plos Genet. 15, e1007935. 10.1371/journal.pgen.1007935. [PubMed: 30668573]

Radeke LJ, and Herman MA (2021). Take a walk to the wild side of *Caenorhabditis elegans*-pathogen interactions. Microbiol. Mol. Biol. R 85.

Rajan M, Anderson CP, Rindler PM, Romney SJ, dos Santos MCF, Gertz J, and Leibold EA (2019). NHR-14 loss of function couples intestinal iron uptake with innate immunity in *C. elegans* through PQM-1 signaling. eLife 8, e44674. 10.7554/eLife.44674. [PubMed: 31532389]

Ritchie ME, Phipson B, Wu D, Hu Y, Law CW, Shi W, and Smyth GK (2015). Limma powers differential expression analyses for RNA-sequencing and microarray studies. Nucleic Acids Res. 43, e47. [PubMed: 25605792]

Robinson MD, McCarthy DJ, and Smyth GK (2010). edgeR: a bioconductor package for differential expression analysis of digital gene expression data. Bioinformatics 26, 139–140. [PubMed: 19910308]

Robinson-Rechavi M, Maina CV, Gissendanner CR, Laudet V, and Sluder A (2005). Explosive lineage-specific expansion of the orphan nuclear receptor HNF4 in nematodes. J. Mol. Evol 60, 577–586. [PubMed: 15983867]

Schoch CL, Seifert KA, Huhndorf S, Robert V, Spouge JL, Levesque CA, Chen W, Consortium FB, List FBCA, Bolchacova E, et al. (2012). Nuclear ribosomal internal transcribed spacer (ITS) region as a universal DNA barcode marker for fungi. Proc. Natl. Acad Sci 109, 6241–6246. [PubMed: 22454494]

Schulenburg H, and Félix MA (2017). The Natural Biotic Environment of Caenorhabditis elegans. Genetics 206, 55–86. 10.1534/genetics.116.195511. [PubMed: 28476862]

Shomer N, Kadhim AZ, Grants JM, Cheng X, Alhusari D, Bhanshali F, Poon AF-Y, Lee MYY, Muhuri A, Park JI, et al. (2019). Mediator subunit MDT-15/MED15 and nuclear receptor HIZR-1/HNF4 cooperate to regulate toxic metal stress responses in *Caenorhabditis elegans*. PLoS Genet. 15, e1008508. [PubMed: 31815936]

Singhvi A, and Shaham S (2019). Glia-neuron interactions in *Caenorhabditis elegans*. Annu. Rev. Neurosci 42, 1–20. [PubMed: 30735460]

Sladek FM (2011). What are nuclear receptor ligands? Mol. Cell Endocrinol 334, 3–13. [PubMed: 20615454]

Taubert S, Ward JD, and Yamamoto KR (2011). Nuclear hormone receptors in nematodes: evolution and function. Mol. Cell Endocrinol 334, 49–55. [PubMed: 20438802]

Troemel ER (2016). Host-microsporidia interactions in *Caenorhabditis elegans*, a model nematode host. Microbiol. Spectr 4. 10.1128/microbiolspec.FUNK-0003-2016.

Visagie CM, Houbraken J, Frisvad JC, Hong S-B, Klaassen CHW, Perrone G, Seifert KA, Varga J, Yaguchi T, and Samson RA (2014). Identification and nomenclature of the genus *Penicillium*. Stud. Mycol 78, 343–371. [PubMed: 25505353]

Wallace BD, and Redinbo MR (2012). Xenobiotic-sensing nuclear receptors involved in drug metabolism: a structural perspective. Drug Metab. Rev 45, 79–100. [PubMed: 23210723]

Wallace SW, Singhvi A, Liang Y, Lu Y, and Shaham S (2016). PROS-1/Prospero is a major regulator of the glia-specific secretome controlling sensory-neuron shape and function in *C. elegans*. Cell Rep. 15, 550–562. [PubMed: 27068465]

Wani KA, Goswamy D, Taubert S, Ratnappan R, Ghazi A, and Irazoqui JE (2021). NHR-49/PPAR-a and HLH-30/TFEB cooperate for *C. elegans* host defense via a flavin-containing monooxygenase. eLife 10, e62775. 10.7554/eLife.62775. [PubMed: 33978570]

Ward JD, Mullaney B, Schiller BJ, He LD, Petnic SE, Couillault C, Pujol N, Bernal TU, Gilst MRV, Ashrafi K, et al. (2014). Defects in the *C. elegans* acyl-CoA synthase, acs-3, and nuclear hormone receptor, nhr-25, cause sensitivity to distinct, but overlapping stresses. Plos One 9, e92552. 10.1371/journal.pone.0092552.eCollection2014. [PubMed: 24651852]

Yuen GJ, and Ausubel FM (2018). Both live and dead *Enterococci* activate *Caenorhabditis elegans* host defense via immune and stress pathways. Virulence 9, 683–699. [PubMed: 29436902]

Zhang J, Holdorf AD, and Walhout AJ (2017). C. **elegans** and its bacterial diet as a model for systems-level understanding of host-microbiota interactions. Curr. Opin Biotechnol 46, 74–80. 10.1016/j.copbio.2017.01.008. [PubMed: 28189107]

Highlights

- The mold *P. brevicompactum* induces XME expression in *C. elegans* gut and glia
- *P. brevicompactum*-dependent XME induction is regulated by *nhr-45* and *nhr-156*
- Failure to induce XMEs in the intestine results in mitochondrial stress and toxicity
- Natural variations in *nhr-156* result in phenotypic diversity in the glial response

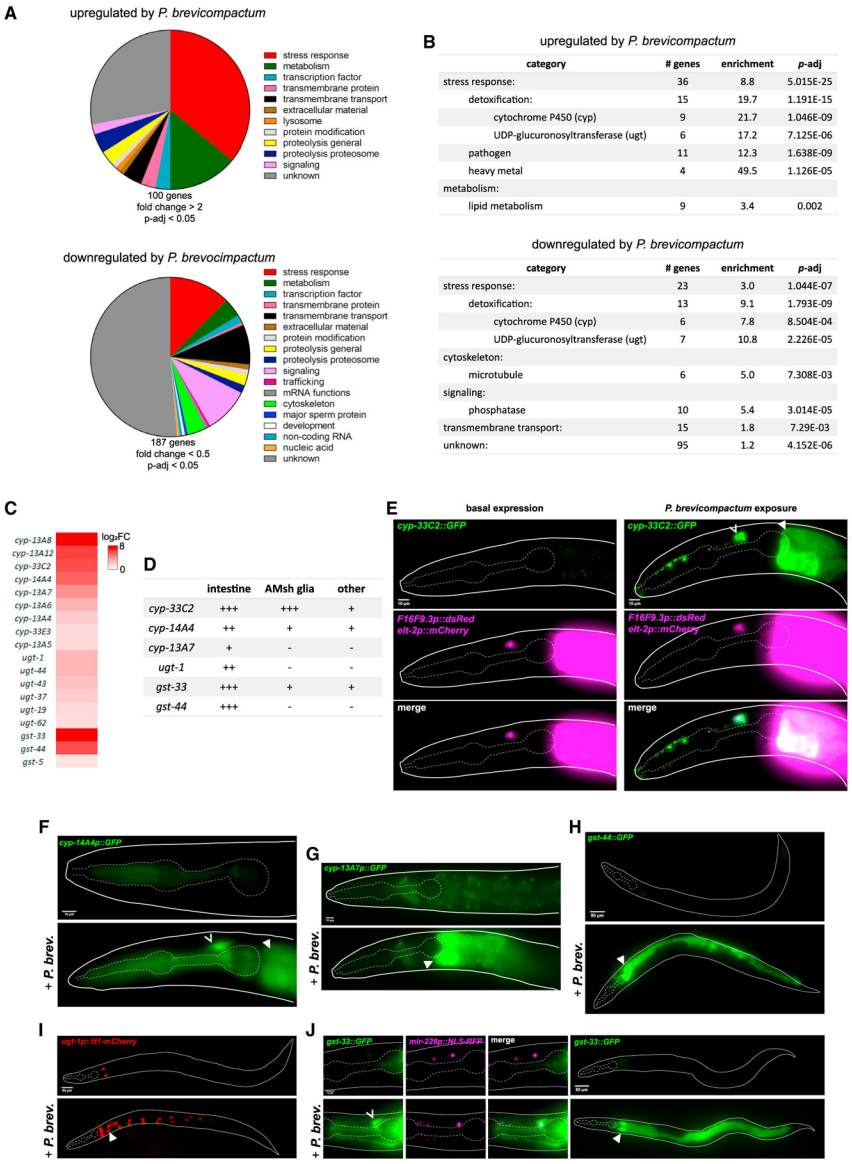

Figure 1. *Penicillium brevicompactum* induces expression of stress response genes including xenobiotic-metabolizing enzymes in *C. elegans*

(A) Classification of *P. brevicompactum*-dependent genes.

(B) Statistically enriched gene categories. (A) and (B) Based on analysis using WormCat (Holdorf et al., 2019).

(C) Heatmap of xenobiotic-metabolizing enzymes (XMEs) induced by *P. brevicompactum*.

(D) Summary of confirmed *P. brevicompactum*-induced genes. +++ strong expression; + + moderate expression; + weak expression. Tissues classified as other are as follows: *cyp-33C2*, excretory cell, vulva, several undefined cells in the head and tail; *cyp-14A4*, pharynx; *gst-33*, excretory cell, pharynx, several undefined cells in the head and tail.

(E) Expression of *cyp-33C2::GFP* with *F16F9.3p::dsRed* (AMsh glia) and *elt-2p::mCherry* (intestine).

(F–J) expression of additional XMEs listed in (D). *mir-228p::NLS-RFP* is pan-glial. Open arrowhead, AMsh glia; closed arrowhead, intestine. All data are based on three biological replicates. Scale bars, 10 μm (E, F, G, and J [left]), 50 μm (H, I, and J [right]).

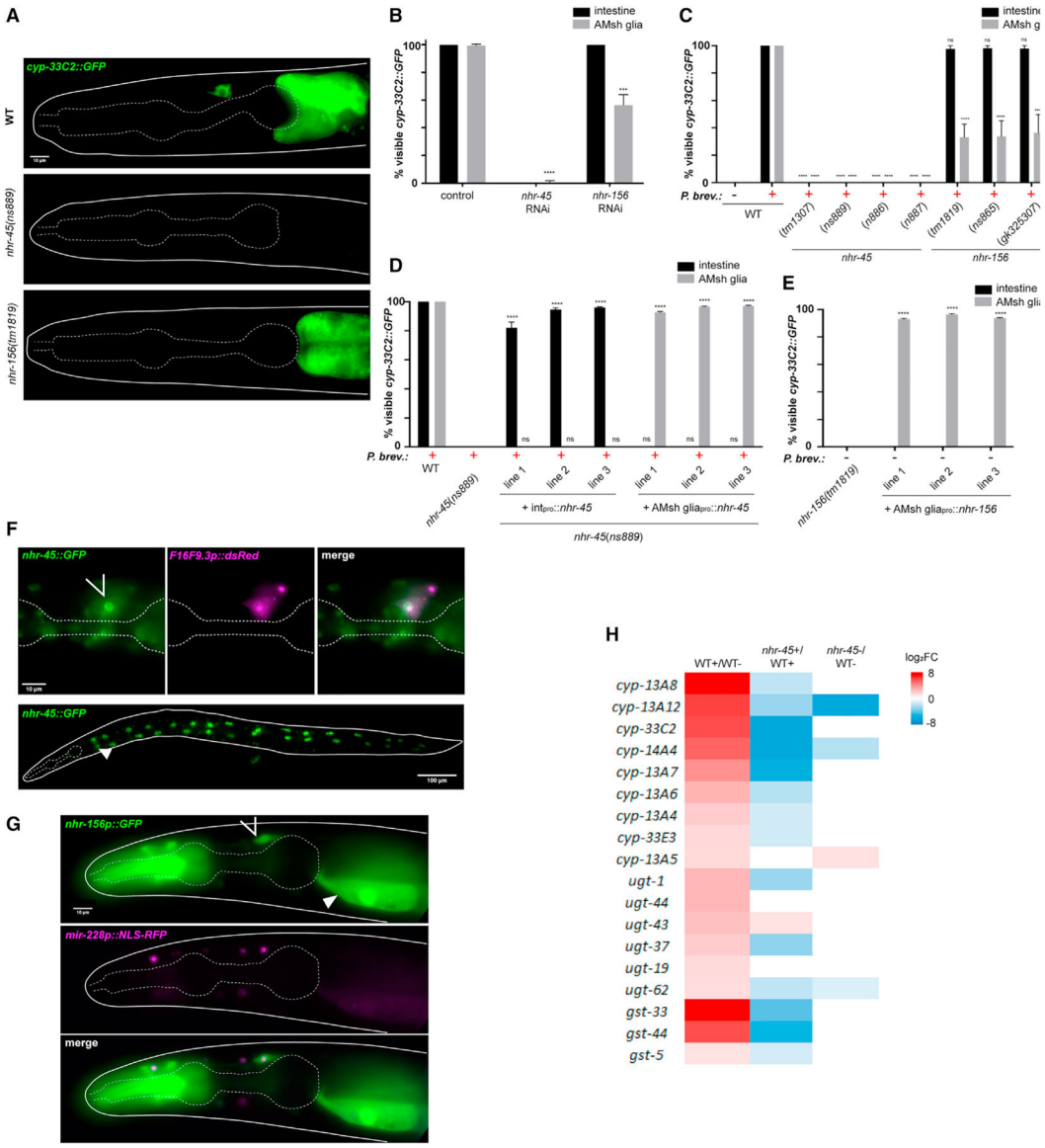

Figure 2. *nhr-45* and *nhr-156* regulate induction of XMEs

(A) *cyp-33C2::GFP* induction following *P. brevicompactum* exposure.

(B) *cyp-33C2::GFP* induction in intestine and AMsh glia in RNAi-treated worms. ****p < 0.0001, ***p < 0.001 (t test). Note that p values cannot be calculated for the intestine because there is no variation between replicates.

(C) *cyp-33C2::GFP* induction in intestine and AMsh glia. *nhr-45 (tm1307)*, 1,545 bp deletion with 235 bp insertion; *nhr-156 (tm1819)*, 553 bp deletion; *nhr-156 (gk325307)*, Trp215 > amber. New alleles generated are as follows: *nhr-45 (ns886)* (14 bp deletion in exon1, generated by CRISPR); *nhr-45 (ns887)* (11 bp insertion in exon 1, generated by CRISPR); *nhr-45 (ns889)* (7 bp deletion in exon 1, generated by CRISPR); *nhr-156 (ns865)* (Gln29 > ochre, generated by EMS mutagenesis). ****p < 0.0001 (ANOVA compared with WT + *P. brevicompactum*).

(D) *cyp-33C2::GFP* induction in intestine and AMsh glia. Int_{pro} is *elt-2p* for intestinal rescue, $AMsh\ glia_{pro}$ is *F16F9.3p* for glial rescue. ****p < 0.0001 (ANOVA compared with *nhr-45[ns889]*).

(E) Basal expression of *cyp-33C2::GFP* in the absence of *P. brevicompactum*. ****p < 0.0001 (ANOVA).

(F) Expression of *nhr-45::GFP* with *F16F9.3p::dsRed* (AMsh glia).

(G) Expression of *nhr-156p::GFP* with *mir-228p::NLS-RFP* (pan-glia). In (F) and (G), open arrow, AMsh glia; closed arrow, intestine.

(H) Heatmap of expression changes of the 18 *P. brevicompactum*-induced XMEs in *nhr-45* partial loss-of-function mutant strain (*nhr-45 [ns889]*; *nsIs910 [elt-2p::nhr-45]*). +, *P. brevicompactum* exposure;−, control samples not exposed. All data are based on three biological replicates. Error bars, SEM (B, C, D, and E). Scale bars, 10 μm (A, F [top], and G), 100 μm (F [bottom]).

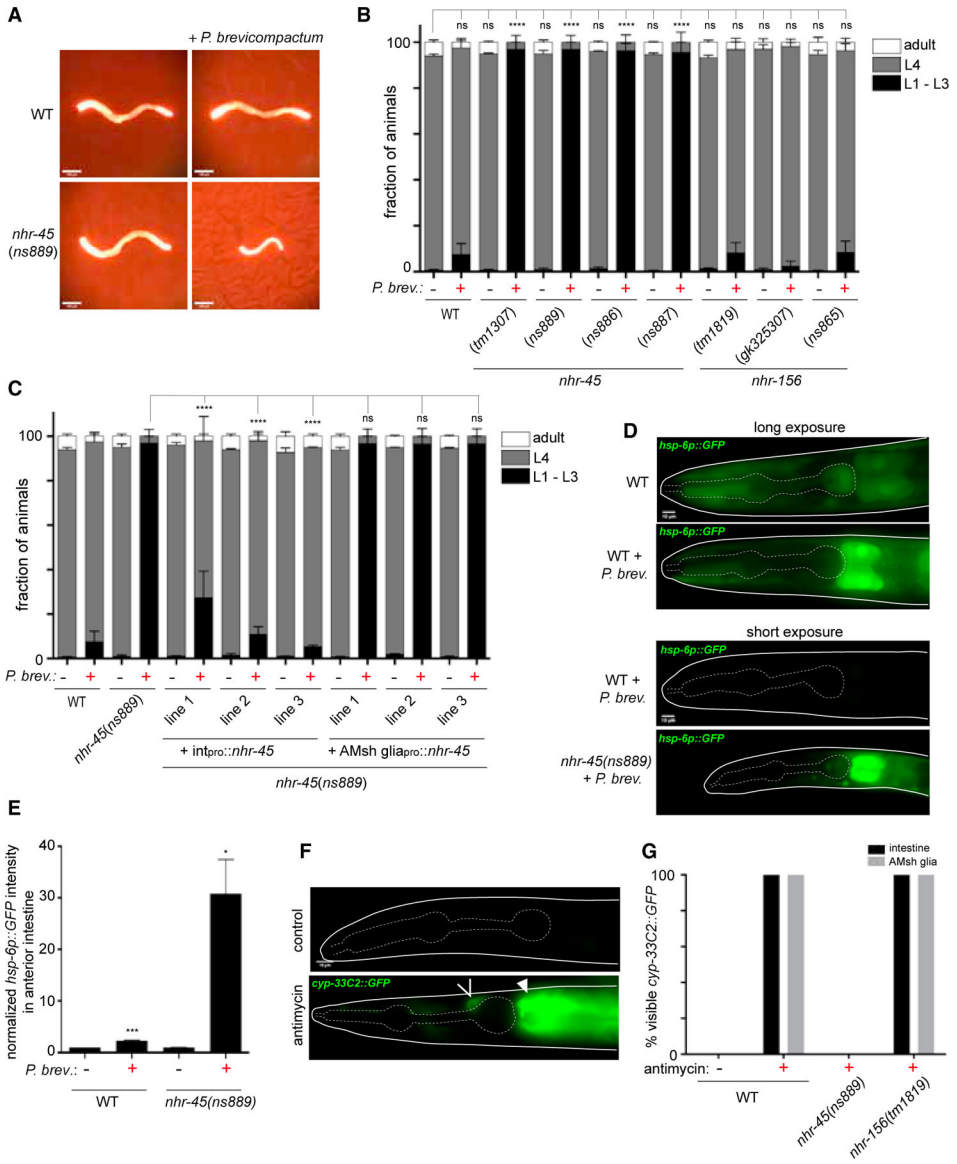

Figure 3. *P. brevicompactum* exposure causes mitochondrial stress and is toxic for *nhr-45* mutants with impaired XME induction

(A) Representative images of indicated strains grown for 2 days from L1 arrest with or without *P. brevicompactum* exposure. *elt-2p::mCherry* is used as a marker to visualize animals.

(B and C) Scoring of developmental stages of indicated strains grown as in (A). (B) ****p < 0.0001 (L4 stage, ANOVA versus WT without *P. brevicompactum*). (C) ****p < 0.0001 (L4 stage, ANOVA versus *nhr-45[ns889]* + *P. brevicompactum*).

(D) *hsp-6p::GFP* expression under the indicated conditions.

(E) Quantification of *hsp-6p::GFP* fluorescence intensity in anterior intestine, normalized to WT without *P. brevicompactum* exposure. ***p < 0.001, *p < 0.05 (t test versus corresponding line without *P. brevicompactum*).

(F) Expression of *cyp-33C2::GFP* following antimycin treatment. Open arrowhead, AMsh glia; closed arrowhead, intestine.

(G) Scoring of *cyp-33C2::GFP* expression in intestine and AMsh glia following antimycin treatment. All data are based on three biological replicates. Error bars, SEM (B and C); SD (E and G). Scale bars, 100 μm (A), 10 μm (D and F).

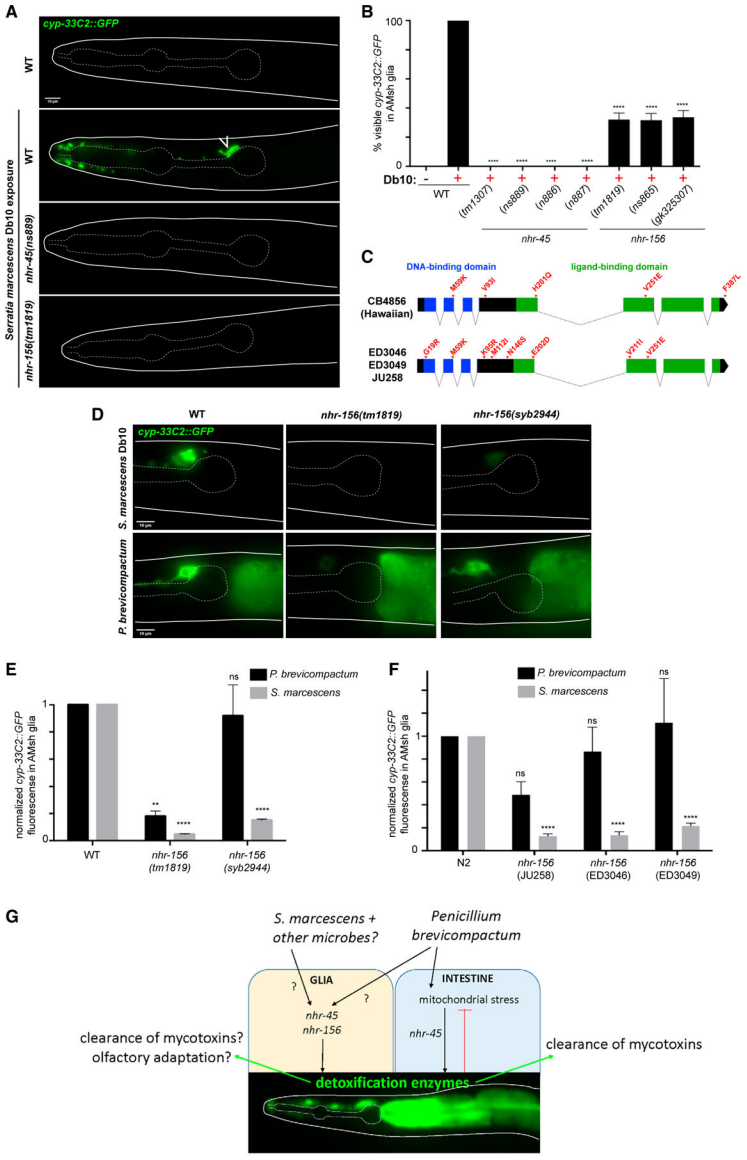

Figure 4. Natural variations in *nhr-156* underlie phenotypic diversity in AMsh glial transcriptional responses to microbes

(A) *cyp-33C2::GFP* expression following *S. marcescens* Db10 exposure. Open arrow, AMsh glia.

(B) Scoring of *cyp-33C2::GFP* induction in AMsh glia. ****p < 0.0001 (ANOVA versus WT + Db10).

(C) Schematic showing SNPs in the *nhr-156* gene that cause amino acid changes.

(D) *cyp-33C2::GFP* expression in AMsh glia following exposure to *S. marcescens* or *P. brevicompactum* in the indicated strains. *syb2944*, WT N2 background with the endogenous *nhr-156* locus replaced with the Hawaiian version of the gene.

(E and F) Quantification of *cyp-33C2::GFP* fluorescence in AMsh glia, normalized to WT for each condition. Genotypes in (F) refer to representative F2 recombinant lines that were generated by crossing *cyp-33C2::GFP* from N2 into the indicated isolates. ****p < 0.0001,

**p < 0.01 (ANOVA versus corresponding WT). All data are based on three biological replicates.

(G) A model for *nhr-45* and *nhr-156* contributions to micorbial responses in *C. elegans*. Error bars, SEM (B); SD (E and F). Scale bars, 10 μm (A and D).

KEY RESOURCES TABLE

REAGENT or RESOURCE	SOURCE	IDENTIFIER
Bacterial and virus strains		
E. coli OP50	CGC	OP50
S. *marcescens* Db10	CGC	Db10
Chemicals, peptides, and recombinant proteins		
Antimycin A from *Streptomyces sp.*	Sigma-Aldrich	A8674
Deposited data		
RNAseq raw data	This study	GEO: GSE183331
Experimental models: Organisms/strains		
Penicillium brevicompactum	ATCC	9056
nsIs775 [pSW81{*cyp-33C2::GFP*} + *elt-2p::mCherry*] I	This study	OS11850
nsIs775 [*cyp-33C2::GFP* + *elt-2p::mCherry*] I; *nsIs143* (*F16F9.3p::dsRed*) X	This study	OS12256
mgIs73 [*cyp-14A4p::GFP::cyp-14A4 3′ UTR* + *myo-2p::mCherry*] V	CGC	GR2250
jrsIs1 [*cyp-13A7p::GFP* + *unc-119(+)*]	CGC	SRU1
stIs11634 [*ugt-1p::H1-mCherry* + *unc-119(+)*]	CGC	RW11634
otEx1182 [*gst-44::GFP* + *rol-6(dom)*]	CGC	OH2204
nsEx5944 [pSW74{*gst-33::GFP*} + *elt-2p::mCherry*]	This study	OS11501
nsEx5944 [pSW74{*gst-33::GFP*} + *elt-2p::mCherry*]; *nsIs698* [*mir-228p::NLS-RFP*]	This study	OS11503
nhr-45 (*tm1307*) X	CGC	VL484
nsIs775 [*cyp-33C2::GFP* + *elt-2p::mCherry*] I; *nhr-45(tm1307)* X	This study	OS12194
nhr-45 (*ns886*) X	This study	OS12363
nsIs775 [*cyp-33C2::GFP* + *elt-2p::mCherry*] I; *nhr-45(ns886)* X	This study	OS12386
nhr-45 (*ns887*) X	This study	OS12364
nsIs775 [*cyp-33C2::GFP* + *elt-2p::mCherry*] I; *nhr-45*(*ns887*) X	This study	OS12387
nhr-45 (*ns889*) X	This study	OS12366
nsIs775 [*cyp-33C2::GFP* + *elt-2p::mCherry*] I; *nhr-45*(*ns889*) X	This study	OS12385
nhr-156 (tm1819) V	NBRP	tm1819
nsIs775 [*cyp-33C2::GFP* + *elt-2p::mCherry*] I; *nhr-156(tm1819) V*	This study	OS12203
nhr-156 (ns865) V	This study	OS12406
nsIs775 [*cyp-33C2::GFP* + *elt-2p::mCherry*] I; *nhr-156(ns865) V*	This study	OS12751
nsIs775 [*cyp-33C2::GFP* + *elt-2p::mCherry*] I; *nhr-156* (*gk325307*)	This study	OS12199
nhr-156 (ns865) V; *nhr-45 (ns889)* X	This study	OS12752
nhr-45 (ns889); nsIs910 [*elt-2p::nhr-45cDNA* + *unc-122p::GFP*]	This study	OS12873
nsIs775 [*cyp-33C2::GFP* + *elt-2p::mCherry*] I; *nhr-45* (*ns889*) X; *nsEx6238* [pSW124{*elt-2p::nhr-45 cDNA*} + *unc-122p::GFP*], gut rescue line 1 of 3	This study	OS12607
nsIs775 [*cyp-33C2::GFP* + *elt-2p::mCherry*] I; *nhr-45*(*ns889*) X; *nsEx6239* [pSW124{*elt-2p::nhr-45 cDNA*} + *unc-122p::GFP*], gut rescue line 2 of 3	This study	OS12608
nsIs775 [*cyp-33C2::GFP* + *elt-2p::mCherry*] I; *nhr-45*(*ns889*) X; *nsEx6240* [pSW124{*elt-2p::nhr-45 cDNA*} + *unc-122p::GFP*], gut rescue line 3 of 3	This study	OS12609
nsIs775 [*cyp-33C2::GFP* + *elt-2p::mCherry*] I; *nhr-45*(*ns889*) X; *nsEx6241* [pSW110 {*F16F9.3p::nhr-45 cDNA*} + *unc-122p::GFP*], glia rescue line 1 of 3	This study	OS12610

REAGENT or RESOURCE	SOURCE	IDENTIFIER
nsIs775 [*cyp-33C2*::*GFP* + *elt-2p*::*mCherry*] I; *nhr-45*(*ns889*) X; *nsEx6242* [pSW110 {*F16F9.3p*::*nhr-45 cDNA*} + *unc-122p*::*GFP*], glia rescue line 2 of 3	This study	OS12611
nsIs775 [*cyp-33C2*::*GFP* + *elt-2p*::*mCherry*] I; *nhr-45* (*ns889*) X; *nsEx6243* [pSW110 {*F16F9.3p*::*nhr-45 cDNA*} + *unc-122p*::*GFP*], glia rescue line 3 of 3	This study	OS12612
nsIs775 [*cyp-33C2*::*GFP* + *elt-2p*::*mCherry*] I; *nhr-156(tm1819)* V; *nsEx6194* [pSW118 {*F16F9.3p*::*nhr-156 cDNA*} + *unc-122p*::*GFP*], glia rescue line 1 of 3	This study	OS12338
nsIs775 [*cyp-33C2*::*GFP* + *elt-2p*::*mCherry*] I; *nhr-156(tm1819)* V; *nsEx6196* [pSW118 {*F16F9.3p*::*nhr-156 cDNA*} + *unc-122p*::*GFP*], glia rescue line 2 of 3	This study	OS12340
nsIs775 [*cyp-33C2*::*GFP* + *elt-2p*::*mCherry*] I; *nhr-156(tm1819)* V; *nsEx6197* [pSW118 {*F16F9.3p*::*nhr-156 cDNA}* + *unc-122p*::*GFP*], glia rescue line 3 of 3	This study	OS12341
nsIs775 [*cyp-33C2*::*GFP* + *elt-2p*::*mCherry*] I; *che-2* (*e1033*) X	This study	OS12903
nsIs775 [*cyp-33C2*::*GFP* + *elt-2p*::*mCherry*] I; *dyf-7* (*m537*) X	This study	OS12094
nsIs775 [*cyp-33C2*::*GFP* + *elt-2p*::*mCherry*] I; *osm-6* (*p811*) V	This study	OS12095
nsIs775 [*cyp-33C2*::*GFP* + *elt-2p*::*mCherry*] I; *tir-1* (*qd4*) III	This study	OS11879
nsIs775 [*cyp-33C2*::*GFP* + *elt-2p*::*mCherry]* I; *sek-1* (*km4*) X	This study	OS12050
nsIs775 [*cyp-33C2*::*GFP* + *elt-2p*::*mCherry*] I; *pmk-1* (*km25*) IV	This study	OS12051
nsIs775 [*cyp-33C2*::*GFP* + *elt-2p*::*mCherry*] I; *nsIs109(F16F9.3p*::*DTA(G53E) + unc-122p*::*GFP)*	This study	OS13492
mgIs73 [*cyp-14A4p*::*GFP*::*cyp-14A4 3′ UTR* + *myo-2p*::*mCherry*] V; *nhr-45* (*ns889*) X	This study	OS13109
mgIs73 [*cyp-14A4p*::*GFP*::*cyp-14A4 3′ UTR* + *myo-2p*::*mCherry*] *nhr-156 (tm1819)* V	This study	OS13110
nsIs143 (*F16F9.3p*::*dsRed*) X; nsEx6176 [WRM0636C_B02 (pRedFlp-Hgr) (nhr-45 [15070]::S0001_pR6K_Amp_2xTY1ce_EGFP_FRT_rpsl_neo_FRT_3xFlagdFRT::unc-119-Nat) + *elt-2p*::*mCherry*]	This study	OS12342
nsIs698 [*mir-228p*::*NLS-RFP*]; *nsEx6179* [pSW121{*nhr-156p*::*GFP*} + *elt-2p*::*mCherry*]	This study	OS12307
zcIs13 [*hsp-6p*::*GFP* + *lin-15(+)*] V	CGC	SJ4100
zcIs13 [*hsp-6p*::*GFP* + *lin-15(+)*] V; *nhr-45* (*ns889*) X	This study	OS13183
nsIs775 [*cyp-33C2*::*GFP* + *elt-2p*::*mCherry*] I; *nhr-156* (*syb2944*) V	This study	OS13345
CB4856 – *C. elegans* Hawaiian isolate	CGC	CB4856
nsIs775 [*cyp-33C2*::*GFP* + *elt-2p*::*mCherry*] I; *nhr-156*(*CB4856*) V	This study	OS13111
JU258 - *C. elegans* wild isolate	CGC	JU258
nsIs775 [*cyp-33C2*::*GFP* + *elt-2p*::*mCherry*] I; *nhr-156* (*JU258)* V	This study	OS13112
ED3046 - *C. elegans* wild isolate	CGC	ED3046
nsIs775 [*cyp-33C2*::*GFP* + *elt-2p*::*mCherry*] I; *nhr-156* (*ED3046*) V	This study	OS13113
ED3049 - *C. elegans* wild isolate	CGC	ED3049
nsIs775 [*cyp-33C2*::*GFP* + *elt-2p*::*mCherry*] I; *nhr-156* (*ED3049*) V	This study	OS13114
JU1088 - *C. elegans* wild isolate	CGC	JU1088
JU1171 - *C. elegans* wild isolate	CGC	JU1171
Recombinant DNA		
pSW81 {*cyp-33C2*pro (1119bp)::*cyp-33C2*::*GFP*::*unc-54 3′ UTR*}	This study	pSW81
pSW74 {*gst-33*pro (907bp)::*gst-33*::*GFP*::*unc-54 3′ UTR*}	This study	pSW74
pSW124 {*elt-2*pro (2908bp)::*nhr-45 cDNA*::*unc-54 3′ UTR*}	This study	pSW124
pSW110 {*F16F9.3*pro (2056bp)::*nhr-45 cDNA*::*unc-54 3′ UTR*}	This study	pSW110
pSW118 {*F16F9.3*pro (2056bp)::*nhr-156 cDNA*::*unc-54 3′ UTR*}	This study	pSW118
pSW121 {*nhr-156*pro (1626bp)::*GFP*::*unc-54 3′ UTR*}	This study	pSW121
WRM0636C_B02 (pRedFlp-Hgr) (nhr-45 [15070] ::S0001_pR6K_Amp_2xTY1ce_EGFP_FRT_rpsl_neo_FRT_3x FlagdFRT::unc-119-Nat)	TransgeneOme	*nhr-45*::*GFP* fosmid